BIOCHEMISTRY
including biophysical chemistry & molecular biology

Article

pubs.acs.org/biochemistry

Kinetic, Mechanistic, and Structural Modeling Studies of Truncated Wild-Type Leucine-Rich Repeat Kinase 2 and the G2019S Mutant

Min Liu,*[,†] Stephanie Kang,[†] Soumya Ray,*[,‡] Justin Jackson,[†] Alexandra D. Zaitsev,[†] Scott A. Gerber,[§] Gregory D. Cuny,[†] and Marcie A. Glicksman[†]

[†]Laboratory for Drug Discovery in Neurodegeneration, Harvard NeuroDiscovery Center, Brigham and Women's Hospital, Harvard Medical School, 65 Landsdowne Street, Fourth Floor, Cambridge, Massachusetts 02139, United States

[‡]Brigham and Women's Hospital, Harvard Medical School, 65 Landsdowne Street, Fourth Floor, Cambridge, Massachusetts 02139, United States

[§]Dartmouth Medical School, One Medical Center Drive, HB-7937, Lebanon, New Hampshire 03756, United States

Supporting Information

ABSTRACT: Leucine-rich repeat kinase 2 (LRRK2), a large and complex protein that possesses two enzymatic properties, kinase and GTPase, is one of the major genetic factors in Parkinson's disease (PD). Here, we characterize the kinetic and catalytic mechanisms of truncated wild-type (t-wt) LRRK2 and its most common mutant, G2019S (t-G2019S), with a structural interpretation of the kinase domain. First, the substitution of threonine with serine in the LRRKtide peptide results in a much less efficient substrate as demonstrated by a 26-fold decrease in k_{cat} and a 6-fold decrease in binding affinity. The significant decrease in k_{cat} is attributed to a slow chemical transfer step as evidenced by the inverse solvent kinetic isotope effect in the proton inventory and pL (pH or pD)-dependent studies. The shape of the proton inventory and pL profile clearly signals the involvement of a general base ($pK_a = 7.5$) in the catalysis with a low fractionation factor in the ground state. We report for the first time that the increased kinase activity of the G2019S mutant is substrate-dependent. Homology modeling of the kinase domain (open and closed forms) and structural analysis of the docked peptide substrates suggest that electrostatic interactions play an important role in substrate recognition, which is affected by G2019S and may directly influence the kinetic properties of the enzyme. Finally, the GTPase activity of the t-G2019S mutant was characterized, and the mutation modestly decreases GTPase activity without significantly affecting GTP binding affinity.

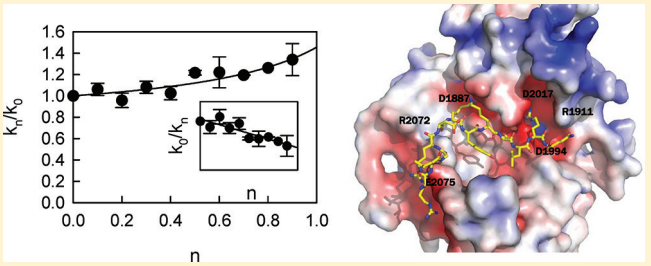

Parkinson's disease (PD), characterized by tremor, rigidity, bradykinesia, and postural instability, is the second most common neurodegenerative disorder after Alzheimer's disease (AD). It affects more than 1 million Americans, and more than 60,000 patients are newly diagnosed each year. PD is caused by a loss of dopaminergic neurons in the *substantia nigra*. Once damaged, these neurons stop producing dopamine, an essential neurotransmitter, and compromise the brain's ability to control movement. Mutations in several genes have been genetically linked to PD in recent years.[1] Among them, leucine-rich repeat kinase 2 (LRRK2) has emerged as the most relevant player in PD pathogenesis. At least 40 mutations in LRRK2 have been identified in the most common familial forms and some sporadic forms of PD and have been associated with typical idiopathic, late-onset PD.[2−6] LRRK2 is a large and complex protein containing several distinct domains, including a leucine-rich repeat (LRR) domain, a Roc domain followed by its associated COR domain, a kinase domain, and a C-terminal WD40 domain.[2,7] LRRK2 is unusual in that it encodes two distinct but functionally linked enzymes: a protein kinase and a GTPase.[7−11] Several lines of evidence have suggested that the kinase activity of LRRK2 plays a critical role in the pathogenesis of PD: (i) several mutations demonstrate increased kinase activity that is correlated with increased neurotoxicity in neurons,[7,12,13] and (ii) kinase inhibitors protect dopaminergic neuron loss in PD animal models.[14] However, most of the LRRK2 mutations do not manifest their effects by simply increasing kinase activity. Even with the considerable debate about the role of LRRK2 kinase activity in the pathogenesis of PD, identification of LRRK2 inhibitors has still become a priority in drug discovery for the treatment of PD. In addition, the identification of LRRK2 inhibitors can provide valuable information for our understanding of LRRK2's functions. Determining the kinetic and catalytic mechanisms of LRRK2 will support structure-based inhibitor design. Herein, we integrate steady-state kinetics with both solvent kinetic isotope effects and molecular modeling studies for both truncated LRRK2 and the most common mutant, G2019S. Specifically, we report results of studies aimed at (i) understanding the

Received: August 1, 2011
Revised: September 8, 2011
Published: September 30, 2011

kinetic and catalytic mechanisms of LRRK2 and (ii) revealing critical structural features of LRRK2.

MATERIALS AND METHODS

Materials. ATP, ADP, AMP-PNP, DTT, magnesium chloride, HEPES, and bovine serum albumin were purchased from Sigma (St. Louis, MO). GTP was from Bioline (Taunton, MA). Peptides LRRKtide (RLGRDKYKTLRQIRQ), LRRKtide^S (RLGRDKYKSLRQIRQ), LRRKtide^A (RLGRDKYKALRQIRQ), and PO_4-LRRKtide [RLGRDKYK(PO$_4$)TLRQIRQ] were purchased from American Peptide (Sunnyvale, CA). PLK-peptide (PLK-derived peptide with an RRRSLLE motif), Eu-anti-phospho-PLK, [γ-^{33}P]ATP, and [α-^{33}P]GTP were from Perkin-Elmer (Boston, MA). Truncated wild-type LRRK2 (amino acids 970−2527) and mutant t-G2019S (amino acids 970−2527) expressed in the baculovirus system were purchased from Invitrogen.

TR-FRET Assay of LRRK2-Catalyzed PLK-Peptide Phosphorylation. The kinase assay for phosphorylation of PLK-peptide (PLK-derived peptide with an RRRSLLE motif) was conducted in buffer containing 20 mM HEPES (pH 7.4), 50 mM NaCl, 10 mM $MgCl_2$, 1 mM DTT, 0.5 mg/mL BSA, 1 mM β-Gly-PO_4, PLK-peptide, and ATP. β-Gly-PO_4 is a phosphatase inhibitor and was added to block phosphatases. PLK-peptide and ATP were used at various concentrations as indicated in Results. The reactions were conducted in duplicate, initiated by the addition of 4 nM LRRK2, and the mixtures were incubated at room temperature for 4 h. The reactions were stopped by the addition of 10 mM EDTA and the mixtures incubated with 2 nM Eu-anti-phospho-PLK for 2 h. The TR-FRET signal was read by an EnVision plate reader (Perkin-Elmer). In all cases, reaction progress curves for production of phospho-PLK-peptide were linear over at last 6 h and allowed calculation of initial velocities.

Kinetic Analysis of LRRK2-Catalyzed LRRKtide and LRRKtide^S Phosphorylation. The kinase assays for phosphorylation of LRRKtide (RLGRDKYKTLRQIRQ) or LRRKtide^S (RLGRDKYKSLRQIRQ) were conducted in buffer containing 20 mM HEPES (pH 7.4), 50 mM NaCl, 10 mM $MgCl_2$, 1 mM DTT, 0.5 mg/mL BSA, 1 mM β-Gly-PO_4, LRRKtide, ATP, and [γ-^{33}P]ATP. Peptidic substrates and ATP were used at various concentrations as indicated in Results, and the ratio of ATP to [γ-^{33}P]ATP was kept constant at all ATP concentrations (250 μM ATP and 5 μCi of [γ-^{33}P]ATP). The reactions were conducted in duplicate, initiated by the addition of 6 nM LRRK2, and the mixtures were incubated at room temperature for 150 min. The reactions were stopped by the addition of 20 mM EDTA, and the mixture was transferred to a multiscreen PH filtration plate (Millipore, Billerica, MA) and washed six times with 75 mM H_3PO_4. The plate was dried; filters were removed, and the samples were counted with a scintillation counter. Background reactions were conducted in the absence of LRRK2. In all cases, reaction progress curves for production of phospho-LRRKtide or phospo-LRRKtide^S were linear over at last 60 min and allowed calculation of initial velocities.

Isotope Exchange Studies of LRRK2-Catalyzed LRRKtide Phosphorylation. [γ-^{33}P]ATP was used as the labeled substrate in these studies, and the rates of exchange of radioactive ATP with PO_4-LRRKtide were measured in buffer containing 20 mM HEPES (pH 7.4), 50 mM NaCl, 10 mM $MgCl_2$, 1 mM DTT, 0.5 mg/mL BSA, and 1 mM β-Gly-PO_4 at several different concentrations of reactants while the concentrations of the other reactants were kept constant. The varied reactants were maintained at a constant ratio of 20. The measurements were repeated for different pairs of reactants. In general, the study was conducted by first mixing all the reactants (ADP, ATP, LRRKtide, and PO_4-LRRKtide) at the desired concentrations. Then a trace amount of [γ-^{33}P]ATP was added before the reaction was initiated by the addition of the enzyme. The exchange reactions were conducted in duplicate, the mixtures incubated at room temperature for 45 min, and the reactions stopped by the addition of 20 mM EDTA. The mixtures were transferred to a multiscreen PH filtration plate (Millipore) and washed six times with 75 mM H_3PO_4. The plates were dried; filters were removed, and the samples were counted with a scintillation counter. Background reactions were conducted in the absence of LRRK2. In all cases, the exchange rate was linear over at least 60 min and allowed calculation of the initial exchange velocity.

Kinetic Analysis of LRRK2-Catalyzed GTP Hydrolysis. The GTPase assay was conducted in buffer containing 20 mM Tris (pH 7.4), 50 mM NaCl, 10 mM $MgCl_2$, 1 mM DTT, 0.5 mg/mL BSA, GTP, and [α-^{33}P]GTP. The reactions were conducted in triplicate, initiated by the addition of 30 nM LRRK2, and the mixtures were incubated at room temperature for 20 min. The reactions were stopped by the addition of 20 mM EDTA, and the product [α-^{33}P]GDP was separated from [α-^{33}P]GTP by PEI-cellulose thin layer chromatography (TLC) (Sigma) developed with 0.5 M KH_2PO_4 (pH 3.4) developing buffer and analyzed with a scintillation counter. In all cases, reaction progress curves for GTP hydrolysis were linear over at least 30 min and allowed calculation of initial velocities.

Mass Spectrometry Analysis of Cysteine Residues Modified with *N*-Ethylmaleimide (NEM). t-wt LRRK2 was treated with 2 mM cysteine-specific inhibitor NEM at room temperature for 30 min. The sample was then reduced with DTT, alkylated with iodoacetamide, and subjected to sodium dodecyl sulfate−polyacrylamide gel electrophoresis for mass spectrometry analysis.

Modeling of the LRRK2 Kinase Domain. The LRRK2 kinase domain between residues 1879 and 2138 was modeled using MODELER.[15] Briefly, the main criteria in homology modeling were template selection and sequence alignment between the target and the template. The top three hits based on sequence identity were yeast snf1 (39% identical), ack1 kinase (33% identical), and B-Raf (33% identical). In this case, the template of B-Raf kinase that had a 33% identical sequence was used for homology modeling because this enzyme had a higher degree of sequence conservation around the ATP binding site region than the other kinases. The Cα root-mean-square deviation (rmsd) and the backbone rmsds for the model and the template crystal structure were <1.0 and <1.2 Å, respectively. The best model was subjected to geometric evaluations using PROCHECK by calculation of the Ramachandran plots.[16] Standard bond lengths and bond angles of the model were determined using WHAT IF[17] with root-mean-square Z scores of 0.889 and 0.91, respectively, suggesting that the model is of high quality. ATP was docked into the binding pocket, and LRRKtide, LRRKtide^S, and PLK were modeled on the basis of the X-ray structures of protein kinase A (PKA) in a complex with a peptidic inhibitor (Protein Data Bank entry 1atp). Individual structues with bound peptides were subjected to 2000 cyles of energy minimization using a steepest descent protocol using DESMOND 3.0

Table 1. Initial Velocity Analysis for LRRK2-Catalyzed Phosphorylation

	LRRKtide		LRRKtide^S		PLK-peptide	
	t-wt	t-G2019S	t-wt	t-G2019S	t-wt	t-G2019S
k_{cat} (min^{-1})	8.1 ± 0.7	17 ± 1.6	0.31 ± 0.06	0.87 ± 0.04	0.018 ± 0.004	0.016 ± 0.001
K_A[a] (μM)	69 ± 6.6	101 ± 16	77 ± 19	161 ± 38	7.1 ± 0.7	10 ± 3.9
K_B[b] (μM)	87 ± 11	79 ± 11	554 ± 187	470 ± 104	0.4 ± 0.05	0.5 ± 0.2
α	1.8 ± 0.1	2.0 ± 0.5	2.6 ± 1.5	0.7 ± 0.2	0.5 ± 0.1	0.6 ± 0.3

[a]A represents ATP. [b]B represents phosphoryl acceptors.

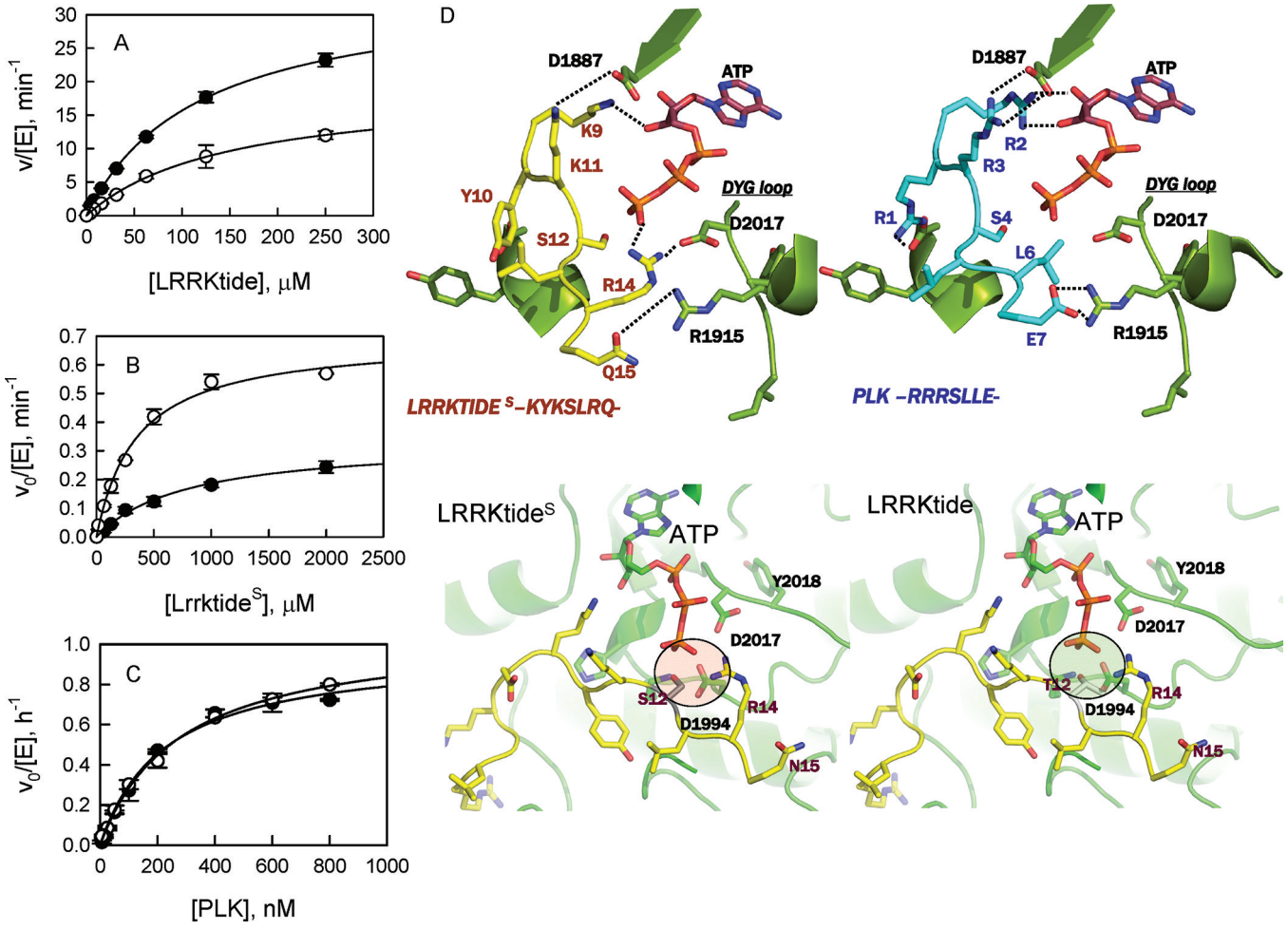

Figure 1. Steady-state kinetic studies of LRRK2-catalyzed phosphorylation. (A) Phosphorylation of LRRKtide by t-wt LRRK2 (○) and the t-G2019S mutant (●). (B) Phosphorylation of LRRKtide^S by t-wt LRRK2 (●) and the t-G2019S mutant (○). (C) Phosphorylation of PLK-peptide by t-wt LRRK2 (●) and the t-G2019S mutant (○). (D) Structural details of peptide binding (LRRKtide at the top left and PLK-peptide at the top right) near the ATP binding site of LRRK2. Both peptides show a series of conserved interactions involving residues such as D1887 and R1915. In the case of LRRKtide, R14 forms hydrogen bonds with ATP as well as D2017 (DGY loop) of LRRK2. The structurally equivalent position in PLK-peptide is occupied by L6 and does not participate in hydrogen bonding with ATP or D2017. This suggests that LRRKtide is likely to be more sensitive to mutations in the DYG loop region than the PLK-peptide. In the bottom left panel, the interaction of LRRKtide^S with the active site of LRRK2 is shown in detail. S12 of LRRKtide^S is in the proximity of charged residues, including D2017 and D1994. In the bottom right panel, the interaction of LRRKtide (contains Thr instead of Ser) with the active site of LRRK2 is shown in detail. The methyl group of T12 is placed between the oxygen of T12 and D1994, leading to charge shielding in this region.

(Schrödinger Inc. and D. E. Shaw Research). The final structures obtained were used for further analysis.

Data Analysis via Basic Equations. Data were analyzed by a nonlinear least-squares method using either Sigma-Plot or Grafit. Standard kinetic mechanisms for two-substrate reactions and their rate equations are shown below:

Ping-pong:

$$v = (k_{cat}[E][A][B])/(K_A[B] + K_B[A] + [A][B]) \quad (1)$$

where K_A and K_B are Michaelis constants.

dx.doi.org/10.1021/bi201173d | Biochemistry 2011, 50, 9399–9408

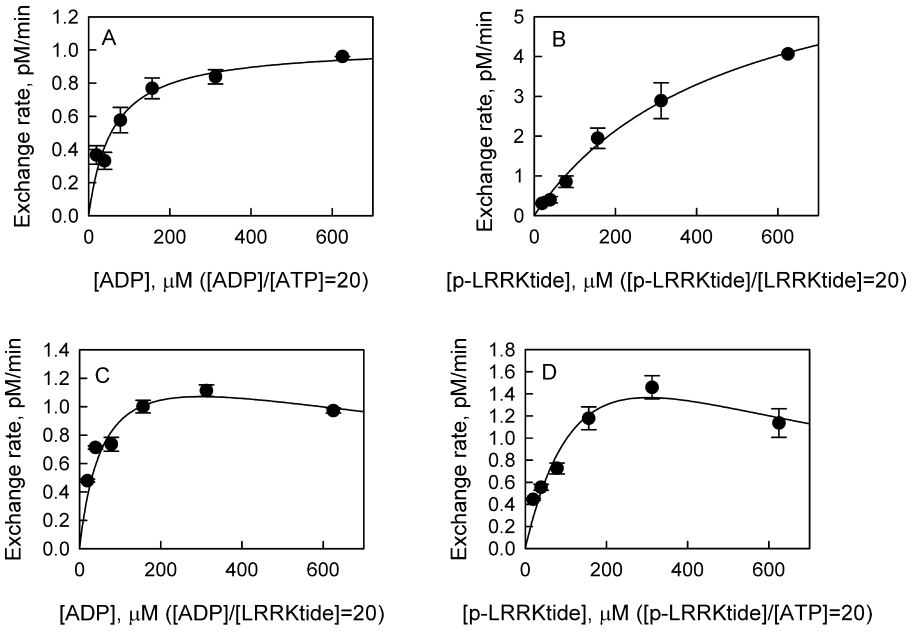

Figure 2. Isotope exchange analysis of t-G2019S mutant-catalyzed LRRKtide phosphorylation. Effect of [ADP]/[ATP] (A), [PO_4-LRRKtide]/[LRRKtide] (B), [ADP]/[LRRKtide] (C), and [PO_4-LRRKtide]/[ATP] (D) ratios on the initial rates of ATP to PO_4-LRRKtide isotopic exchange. The concentrations of the varied reactants were maintained at a constant ratio of 20 while the concentrations of the other reactants were kept at 1 and 20 μM for the substrate and product, respectively. The trace amount of radioactive ATP was added prior to the initiation of the reaction by the addition of enzyme. The data in panels A and B were fit to the simple Michaelis−Menten equation, and the data in panels C and D were fit to the equation reflecting the substrate inhibition $\{v = v_{max}[S]/[K_m + [S](1 + [S]/K_i)]\}$.

Rapid equilibrium ordered:

$$v = (k_{cat}[E][A][B])/(K_A K_B + K_B[A] + [A][B]) \quad (2)$$

where K_A and K_B are substrate dissociation constants for EA and EB, respectively.

Rapid equilibrium random/steady-state ordered:

$$v = (k_{cat}[E][A][B])/(\alpha K_A K_B + \alpha K_A[B] + \alpha K_B[A] + [A][B]) \quad (3)$$

For rapid equilibrium systems, K_A, K_B, αK_A, and αK_B are substrate dissociation constants for EA, EB, and EAB; for steady-state systems, K_A is the substrate dissociation constant for EA and αK_A and αK_B are Michaelis constants. For definitions of mechanisms, substrate dissociation constants, and α, see ref 18.

RESULTS

Initial Velocity Studies of the t-wt LRRK2- and Mutant t-G2019S-Catalyzed Phosphorylation of LRRKtide. To determine the kinetic mechanism for the phosphorylation of LRRKtide (RLGRDKYKTLRQIRQ), we measured initial velocities as a function of LRRKtide concentration at several fixed concentrations of ATP for t-wt LRRK2 and the t-G2019S mutant (see Figure S1 of the Supporting Information). The complete data sets were subjected to global analysis by nonlinear least-squares fits to the three standard mechanisms (ping-pong, rapid equilibrium order, and rapid equilibrium random/steady-state ordered) using eqs 1−3. Statistically, the data fit the random mechanism (or steady-state ordered mechanism) the best for both t-wt LRRK2 and the t-G2019S mutant, yielding the following estimates averaged from two independent experiments: k_{cat} = 8.1 ± 0.7 min^{-1}, K_{ATP} = 69 ± 6.6 μM, $K_{LRRKtide}$ = 87 ± 11 μM, and α = 1.8 ± 0.1 for t-wt LRRK2; k_{cat} = 17 ± 1.6 min^{-1}, K_{ATP} = 101 ± 16 μM, $K_{LRRKtide}$ = 79 ± 11 μM, and α = 2.0 ± 0.5 for the mutant t-G2019S, as summarized in Table 1. The t-G2019S mutant increases the k_{cat} by 2-fold without significantly affecting the binding affinity of ATP and LRRKtide. A direct comparison of the t-G2019S mutant with t-wt LRRK2 is shown in Figure 1A, where the initial velocities were measured as a function of LRRKtide concentration at a saturating concentration of ATP.

Initial Velocity Studies of LRRK2-Catalyzed LRRKtide^S Phosphorylation. Peptide LRRKtide^S (RLGRDKYKSLRQIRQ) was derived from LRRKtide, in which the phosphorylatable threonine was replaced with a serine residue. The initial velocities were measured as a function of LRRKtide^S concentration, at several fixed concentrations of ATP for t-wt LRRK2 and the t-G2019S mutant (see Figure S2 of the Supporting Information). Statistically, the data fit the random mechanism (or steady-state ordered mechanism) the best for both t-wt LRRK2 and the t-G2019S mutant. The kinetic parameter estimates averaged from two independent experiments were generated: k_{cat} = 0.31 ± 0.06 min^{-1}, K_{ATP} = 77 ± 19 μM, $K_{LRRKtide^S}$ = 554 ± 187 μM, and α = 2.6 ± 0.5 for t-wt LRRK2; k_{cat} = 0.87 ± 0.04 min^{-1}, K_{ATP} = 161 ± 38 μM, $K_{LRRKtide^S}$ = 470 ± 104 μM, and α = 0.7 ± 0.2 for the t-G2019S mutant (as summarized in Table 1). A direct comparison of the phosphorylation of LRRKtide^S by the t-G2019S mutant and t-wt LRRK2 is shown in Figure 1B, where the initial velocities were measured as a function of LRRKtide^S concentration at a saturating concentration of ATP.

Initial Velocity Studies of t-wt LRRK2- and Mutant t-G2019S-Catalyzed Phosphorylation of PLK-Peptide. A TR-FRET assay has been developed for measuring the phosphorylation of PLK-peptide (a motif of RRRSLLE). Previously, the reaction was evaluated using a radiometric assay, and the linear correlation between the FU and

nanomolar units allowed the conversion of initial velocities from FU per hour to nanomolar per hour.[19] To determine the kinetic mechanism of t-wt LRRK2- and mutant t-G2019S-catalyzed phosphorylation of PLK-peptide, initial velocities were measured over a range of ATP concentrations at several fixed concentrations of PLK-peptide (see Figure S3 of the Supporting Information). The data fit the random (or steady-state ordered) mechanism the best for both t-wt LRRK2 and the t-G2019S mutant, yielding the following estimates averaged from two independent experiments: k_{cat} = 0.018 ± 0.004 min^{-1}, K_{ATP} = 7.1 ± 0.7 μM, $K_{PLK\text{-}peptide}$ = 0.43 ± 0.05 μM, and α = 0.5 ± 0.1 for t-wt LRRK2; k_{cat} = 0.016 ± 0.001 min^{-1}, K_{ATP} = 10 ± 3.9 μM, $K_{PLK\text{-}peptide}$ = 0.5 ± 0.2 μM, and α = 0.6 ± 0.3 for the t-G2019S mutant (as summarized in Table 1). Unlike the results for LRRKtide and LRRKtide^S, the t-G2019S mutant exhibits activity similar to that of t-wt LRRK2. The t-G2019S mutant also had little effect on the binding affinity of ATP and PLK-peptide. A direct comparison of the phosphorylation of PLK-peptide by the t-G2019S mutant and t-wt LRRK2 is shown in Figure 1C, where the initial velocities were measured as a function of PLK-peptide concentration at a saturating concentration of ATP.

Isotope Exchange and Product Inhibition Studies for t-wt LRRK2- and Mutant t-G2019S-Catalzyed LRRKtide Phosphorylation. Attempts to measure the rate of exchange of radioactive ATP with PO_4-LRRKtide at equilibrium were not successful because of the inaccurate determination of the equilibrium constant of the reaction. To keep the system the same distance from equilibrium under all the conditions, the concentrations of the varied reactants were maintained at a constant ratio while the other reactant concentration was kept constant.[18] The concentrations of the varied reactants were kept at a ratio of 20 ([product]/[substrate] = 20), while the concentrations of the other reactants were kept at 1 and 20 μM for the substrate and product, respectively. The exchange was initiated by the addition of the enzyme. The effects of increasing concentrations of the varied reactants on exchange rates were tested for both t-wt LRRK2 and the t-G2019S mutant. First, in all cases, the exchange was linear for at least 60 min (see Figure S4 of the Supporting Information) and was stopped after incubation for 45 min, which allowed the calculation of the initial exchange rate. Next, the initial exchange rate was tested as a function of enzyme concentration and found to be linearly proportional to the enzyme concentration (see Figure S5 of the Supporting Information). Finally, the effects of increasing concentrations of reactants on the initial rate of exchange of radioactive ATP with PO_4-LRRKtide were examined. For the t-G2019S mutant, increasing the concentrations of structurally related reactants (i.e., ADP/ATP or PO_4-LRRKtide/LRRKtide) resulted in increased rates of exchange of ATP with PO_4-LRRKtide (Figure 2A,B). However, substrate inhibition was observed when structurally unrelated reactants (i.e., PO_4-LRRKtide/ATP or ADP/LRRKtide) were varied: the exchange rate initially increased with an increasing reactant concentration and gradually and partially decreased (Figure 2C,D). Identical patterns were revealed for t-wt LRRK2 as summarized in Table 2. These patterns are consistent with a random mechanism for both t-wt LRRK2 and the t-G2019S mutant with the abortive complex formed, i.e., E−ADP−LRRKtide or E−ATP−PO_4-LRRKtide.

The product inhibition studies were also conducted with products ADP and PO_4-LRRKtide (see Figure S6 of the Supporting Information). For t-G2019S mutant-catalyzed LRRKtide phosphorylation, symmetric inhibition patterns were revealed; ADP was competitive with ATP and non-competitive with LRRKtide, and PO_4-LRRKtide was competitive with LRRKtide and noncompetitive with ATP as summarized in Table 3. These product inhibition patterns are also consistent with a rapid equilibrium random mechanism with E−PO_4-LRRKtide−ATP and E−LRRKtide−ADP abortive complexes formed. Identical inhibition patterns were revealed for t-wt LRRK2.

Table 2. Isotope Exchange Analysis for t-wt LRRK2- and t-G2019S Mutant-Catalyzed LRRKtide Phosphorylation

		substrate-product pair[a]			
	exchange	A-Q	B-Q	B-P	A-P
t-wt	ATP−PO_4-LRRKtide	H[b]	HPD[c]	H[b]	HPD[c]
t-G2019S	ATP−PO_4-LRRKtide	H[b]	HPD[c]	H[b]	HPD[c]

[a]A represents ATP. B represents LRRKtide. P represents PO_4-LRRKtide. Q represents ADP. [b]Hyperbolic. [c]Hyperbolic with partial depression.

Inhibition Studies of t-wt LRRK2- and t-G2019S Mutant-Catalyzed LRRKtide^S and PLK-Peptide Phosphorylation. The kinetic mechanism of t-wt LRRK2- and t-G2019S mutant-catalyzed PLK-peptide and LRRKtide^S phosphorylation was determined by conducting the inhibition studies using substrate analogues AMP-PNP and LRRKtide^A (RLGRDKYKALRQIRQ), in which the phosphorylatable threonine was replaced with alanine. Symmetric inhibition patterns were revealed for all the reactions as summarized in Table 3, suggesting that both t-wt LRRK2 and the t-G2019S mutant follow a random mechanism for the phosphorylation of PLK-peptide and LRRKtide^S.

Proton Inventory Studies. The proton inventory studies of both t-wt LRRK2- and t-G2019S mutant-catalyzed phosphorylation of LRRKtide were conducted to determine k_{cat} (initial velocity measured at saturating concentrations of both ATP and LRRKtide) in a mixture of H_2O and D_2O at pH 8.2 and an equivalent pD. The dependence of the ratio of k_{cat} (k_n/k_0) in the presence and absence of varying atom fractions of D_2O (n) on n is presented in Figure 3A for t-wt LRRK2-catalyzed LRRKtide phosphorylation. The solvent deuterium isotope effect on k_{cat} can be expressed by the Gross−Butler equation:[20]

$$k_n/k_0 = (1 - n + n\phi^T)/(1 - n + n\phi^R) \quad (4)$$

where ϕ^R and ϕ^T are fractionation factors for the exchangeable hydrogen in the reactant and transition states, respectively. Fitting the data in Figure 3A to the equation gives the following estimates: ϕ^R = 1, and ϕ^T = 1.03. Given this, we can assign the estimate to the solvent kinetic isotope effect (SKIE) on k_{cat}: $^D k_{cat} = \phi^R/\phi^T$ = 1.1 ± 0.1 for t-wt LRRK2 (determined from three independent experiments). A similar proton inventory was observed on k_{cat} for t-G2019S mutant-catalyzed LRRKtide phosphorylation, and a SKIE of 1.2 ± 0.2 was determined from three independent experiments.

Proton inventory studies of LRRKtide^S phosphorylation were also conducted to determine k_{cat} (initial velocities measured for both ATP and LRRKtide^S at saturating concentrations) for both t-wt and the t-G2019S mutant. Figure 4A shows the dependence of the ratio of k_{cat} (k_n/k_0) on atom fractions of D_2O (n) in the presence and absence of varying D_2O concentrations for t-wt LRRK2. The plot revealed a nonlinear

Table 3. Inhibition of the t-G2019S Mutant by Substrate Analogues and Products

inhibitor	substrate	mechanism	$K_{i,e}$ (mM)	$K_{i,ea}$ (mM)	$K_{i,eb}$ (mM)
ADP	ATP	C	0.1 ± 0.02		
	LRRKtide	NC	0.3 ± 0.03		0.1 ± 0.01
PO_4-LRRKtide	ATP	NC	2.1 ± 0.3	1.7 ± 0.1	
	LRRKtide	C	1.8 ± 0.1		
AMP-PNP	ATP	C	0.4 ± 0.2		
	LRRKtide^S	NC	1.3 ± 0.3		1.3 ± 0.2
LRRKtide^A	ATP	NC	0.8 ± 0.3	0.5 ± 0.1	
	LRRKtide^S	C		0.5 ± 0.1	
AMP-PNP	ATP	C	0.4 ± 0.2		
	PLK-peptide	NC	1.3 ± 0.3		1.3 ± 0.2
LRRKtide^A	ATP	NC	0.8 ± 0.3	0.5 ± 0.1	
	PLK-peptide	C		0.5 ± 0.1	

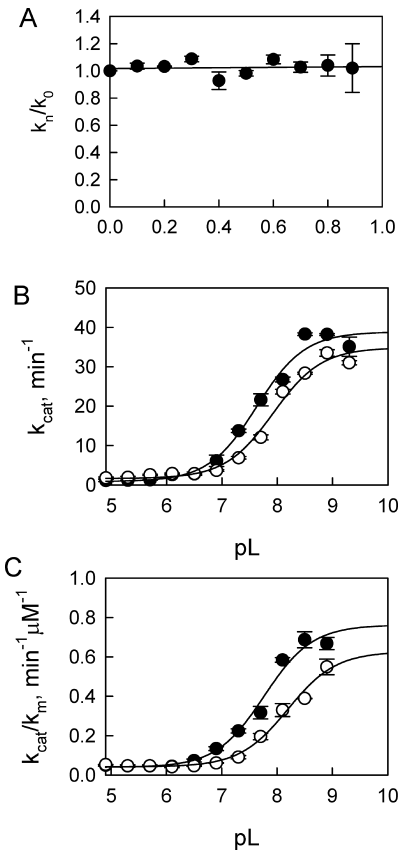

Figure 3. Proton inventory and pL-dependent studies of t-wt LRRK2-catalyzed LRRKtide phosphorylaiton. For the proton inventory study, the initial velocities were measured at saturating concentrations of both ATP and peptide substrates for k_{cat} in a mixture of H_2O and D_2O at pH 8.2 and an equivalent pD. The dependence of the ratio of k_{cat} (k_n/k_0) in the presence and absence of varying atom fractions of D_2O (n) on n revealed a normal SKIE of 1.1 (A). pL-dependent studies were conducted using a triple buffer consisting of 50 mM MES, 100 mM Tris, and 50 mM acetic acid. Panel B revealed pH (●) and pD (○) dependencies of k_{cat} with a SKIE of 1.1, and panel C revealed pH (●) and pD (○) dependencies of k_{cat}/K_m with a SKIE of 1.2.

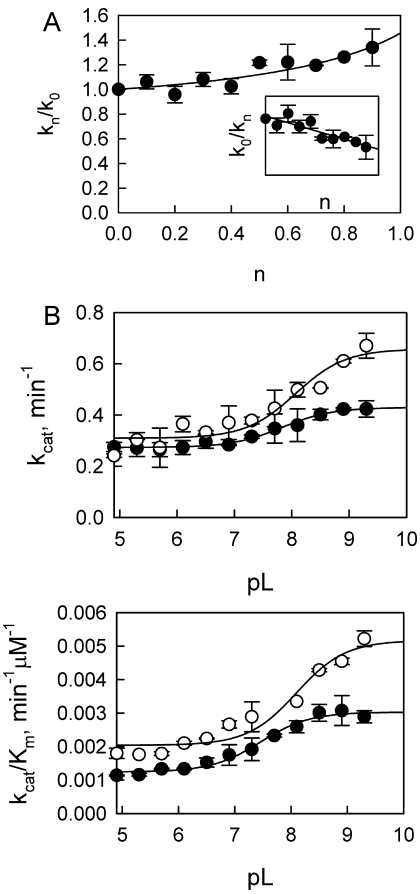

Figure 4. Proton inventory and pL-dependent studies of t-wt LRRK2-catalyzed LRRKtide^S phosphorylation. Panel A shows proton inventory studies of LRRKtide^S phosphorylation. The inset shows the dependence of the reciprocal of the ratio of k_{cat} (k_0/k_n) on n. Panel B reveals pH (●) and pD (○) dependencies of k_{cat} with a SKIE of 0.65, and panel C reveals pH (●) and pD (○) dependencies of k_{cat}/K_m with a SKIE of 0.57.

dependence of k_n/k_0 on n and was fit to eq 4 well, yielding the following estimates: $\phi^T = 1$, and $\phi^R = 0.7$. Given this, we can assign the estimate to the SKIE for k_{cat} ($^Dk_{cat} = \phi^R/\phi^T = 0.7$) and also expect that the reciprocal of the equation should be linear in terms of n. The inset of Figure 4A shows that this expectation is met [the reciprocal of the ratio of k_{cat} (k_0/k_n) linearly depends on n]. A similar proton inventory was observed on k_{cat} for t-G2019S mutant-catalyzed LRRKtide^S phosphorylation, and an inverse SKIE of 0.7 ± 0.1 was determined from three independent experiments.

pL Dependence of Steady-State Kinetic Parameters and SKIE. The steady-state kinetic parameter pL (pH or pD) profile of LRRKtide^S phosphorylation was conducted in a triple buffer consisting of 50 mM MES, 100 mM Tris, and 50 mM acetic acid along with other components as described in Materials and Methods. The combination of the three buffers

dx.doi.org/10.1021/bi201173d | Biochemistry 2011, 50, 9399–9408

has the advantage of providing a constant ionic strength for the entire pL range studied. The pH stability of LRRK2 was determined by incubating the enzyme at the desired pH and assaying aliquots at pH 7.5. The enzyme was determined to be stable from pH 6 to 9.3. A small activity loss occurs at pH <5.5. However, the small activity loss does not affect the measurement of initial velocities, because the enzyme was added from a stock solution at pH 7.5 to the reaction mixture and assayed for 30 min in the presence of substrate, which is likely to provide some protection against denaturation. The LRRK2-catalyzed phosphorylation of LRRKtide^S was monitored in a pL range of 4.9−9.3 for k_{cat} (initial velocities measured at saturating ATP and LRRKtide^S concentrations of 1 and 2 mM, respectively) and for k_{cat}/K_m (initial velocities measured at ATP and LRRKtide^S concentrations 10-fold lower than the K_m values, 10 and 50 μM, respectively). The pL profile of k_{cat} for t-wt LRRK2 revealed an acidic limb (Figure 4B) and was fit to eq 5, yielding apparent pK_a values of 7.7 and 8.2 from pH and pD profiles, respectively.

$$y = \frac{C}{1 + 10^{-\mathrm{pH}}/10^{-\mathrm{p}K_a}} \quad (5)$$

k_{cat}/K_m exhibited a pL dependence similar to that of k_{cat}, revealing apparent pK_a values of 7.5 and 8.0 from pH and pD profiles, respectively (Figure 4C). The pL-independent steady-state parameters revealed SKIE values of 0.65 and 0.57 for k_{cat} and k_{cat}/K_m, respectively. Similar pL profile and SKIE values were observed for the t-G2019S mutant (see Figure S7 of the Supporting Information).

The same pL-dependent studies were conducted for LRRKtide, as well. The pL profiles revealed similar shapes with apparent pK_a values of 7.6 and 7.9 from pH and pD profiles, respectively, for k_{cat} and apparent p$K_a$values of 7.7 and 8.2 from pH and pD profiles, respectively, for k_{cat}/K_m (Figure 3B,C). The pL-independent steady-state parameters revealed SKIE values of 1.1 and 1.2 for k_{cat} and k_{cat}/K_m, respectively. Similar pL profile and SKIE values were observed for the t-G2019S mutant (see Figure S8 of the Supporting Information).

Mass Spectrometry Analysis of Cysteine Residues Modified with *N*-Ethylmaleimide (NEM). Mass spectrometry analysis revealed 28 cysteine residues modified by NEM. Twenty-three of them are located in the LRR, COR, and WD40 domains. Only one cysteine, C1465, is in the GTPase domain, and four (C2024, C2025, C2101, and C2114) are in the kinase domain.

Steady-State Kinetic Study of LRRK2-Catalyzed Hydrolysis of GTP. To characterize LRRK2-catalyzed hydrolysis of GTP, a radiometric assay in which [α-^{33}P]GDP is separated from [α-^{33}P]GTP by TLC and counted with a scintillation counter was developed. The production of GDP is linearly dependent on both time and enzyme concentration (data not shown). Initial velocities were measured as a function of GTP concentration for t-wt and the t-G2019S mutant (Figure 5). The dependence of initial velocities on GTP concentration adheres to the simple Michaelis−Menten equation, which allowed us to calculate the steady-state kinetic parameters: k_{cat} = 0.04 ± 0.004 s^{-1} and K_{GTP} = 0.7 ± 0.1 mM for t-wt LRRK2; k_{cat} = 0.03 ± 0.002 s^{-1} and K_{GTP} = 0.4 ± 0.1 mM for the t-G2019S mutant. These results suggest that the mutation decreases the GTPase activity by 20% without significantly affecting the binding of GTP.

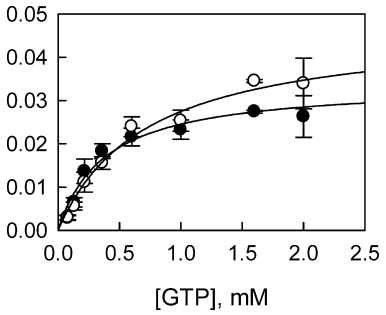

Figure 5. LRRK2-catalyzed GTP hydrolysis. Initial velocities were measured as a function of GTP concentration for t-wt LRRK2 (○) and the t-G2019S mutant (●).

Modeling of the LRRK2 Kinase Domain. The LRRK2 kinase domain between residues 1879 and 2138 was modeled using MODELER[15] (details in Materials and Methods). ATP was docked into the ATP-binding pocket using GLIDE,[21,22] and the final model in complex with peptide substrates is shown in Figure 1D and Figure S9 of the Supporting Information. The LRRK2 kinase model shows all of the expected subdomains of a Ser/Thr protein kinase (see Figure S9c of the Supporting Information).[23−26] The ATP binding cleft shows a glycine-rich loop (residues 1885−1982) facilitating interactions of the backbone with the γ-phosphate of ATP (see Figure S9c of the Supporting Information).[27] D2017 is part of the regulatory DYG loop and makes a stabilizing interaction with ATP via the Mg^{2+} ion.[25,26] The DYG loop in this case was modeled on the "DYG-in" active form of the kinase. In addition, the catalytic loop shows H1998, K1996, and D1995 correctly positioned for catalysis in the proximity of the γ-phosphate of ATP. The LRRK2 kinase domain shows spatial conservation of residues in the regulatory spine like other kinases in this subfamily[25] and comprises residues L1924, L1935, Y1992, and Y2018. The catalytic spine comprises V1893, L1955, L2001, L2062, and I2066. The adenine group of the ATP molecules completes this catalytic spine by positioning itself between V1893 and L2001. In addition, the model shows C2024 and C2025, which are both on the regulatory loop, exposed to solvent.

DISCUSSION

Source of LRRK2 Enzymes. We have reported the characterization of the kinase and GTPase activities of full-length mouse wt LRRK2 purified from mouse brain.[19] Because of the difficulty in generating the full-length G2019S mutant, for this study, we used the truncated version of human LRRK2 and the G2019S mutant containing residues 970−2527, which includes the Roc, COR, kinase, WD40, and entire C-terminal domains expressed in the baculovirus system. The truncated protein demonstrated both kinase and GTPase activities.

Initial Velocity Studies Revealed That the t-G2019S Mutant Increases the Kinase Activity in a Substrate-Dependent Manner. The natural substrates of LRRK2 are not known. Several potential substrates of LRRK2 have been described, including ezrine, radixin, and moesin (ERM), eukaryotic initiation factor 4E (eIF4E)-binding protein (4E-BP), MAPK kinases, β-tubulin, and α-synuclein.[28−32] However, none of the proteins has proven to be efficiently phosphorylated by LRRK2 in cells or animals. Therefore, in this study, LRRKtide and PLK-peptide were used as phosphoryl acceptors.

dx.doi.org/10.1021/bi201173d | *Biochemistry* 2011, 50, 9399−9408

The G2019S mutant has been consistently reported to increase the kinase activity of LRRK2 by 2−3-fold.[7,8,11,33] In this study, we were able to replicate this finding for LRRKtide phosphorylation. However, when PLK-peptide was used as the phosphoryl acceptor, surprisingly the t-G2019S mutant exhibited no difference in specific activity versus that of t-wt LRRK2. It has been reported that LRRK2 favors threonine over serine for phosphorylation. Replacement of threonine with serine in the Nictide peptide abolished phosphorylation by LRRK2.[34] The lack of increased activity of the t-G2019S mutant might be attributed to the unfavorable serine residue. Therefore, the LRRKtide^{S} peptide in which phosphorylatable threonine was replaced with serine was prepared. The replacement resulted in a much less efficient substrate. This is most likely due to a possible charge repulsion introduced by serine that weakens the electrostatic network between LRRK2 and the peptide substrate (Figure 1D; also see the Supporting Information for details). However, the t-G2019S mutant still retains a 3-fold increase in k_{cat} compared to that of t-wt LRRK2.

Modeling the LRRK2 kinase domain in complex with ATP, LRRKtide$^{(T/S)}$, and/or PLK-peptide provides a system for understanding the substrate-dependent effect of the t-G2019S mutant (Figure 1D). PLK-peptide has a higher charge density with excellent charge complementarity with the nearby LRRK2 substrate binding pocket (see the Supporting Information for details) and is consistent with >200-fold tighter binding of the PLK-peptide relative to that of LRRKtide, as demonstrated by differences in K_m values (a K_m of 0.4 μM for PLK-peptide vs a K_m of 87 μM for LRRKtide). The tight binding of the PLK-peptide minimizes any effect that the t-G2019S mutant may have, therefore eliminating any difference between t-wt LRRK2 and the t-G2019S mutant. The individual interactions between peptide substrates and LRRK2 will be tested by making a series of single-amino acid changes in a future study.

The observation that the t-G2019S mutant exhibits a substrate-dependent effect on kinase activity highlights the uncertainty about whether the G2019S mutant will necessarily have increased kinase activity toward physiological substrates compared to wt LRRK2. The fact that most of the LRRK2 mutations do not simply increase kinase activity, along with our observation of the t-G2019S mutant, raises the possibility that there might be complex mechanisms that regulate the functions and enzymatic activities of the G2019S mutant and other mutants. A more comprehensive understanding of the effects of LRRK2 mutations must take into account the complex mechanisms that regulate LRRK2's functions. The recent discovery of 14-3-3[33] has begun to reveal the mutant-specific regulating mechanisms of LRRK2.

Formation of a Nonproductive Complex and Its Impact on Inhibitor Efficacy in Vivo. Values of K_{ATP} for the reaction of LRRK2 with PLK-peptide and LRRKtide/LRRKtide^{S} dramatically depend on the identity of the phosphoryl acceptor with a notable difference of 10-fold. Given an α value of 2 versus an α value of 0.5, this difference in K_{ATP} is large. As discussed in more detail previously,[35] a mechanism that involves the formation of a nonproductive binary complex upon the binding of the phosphoryl acceptor to free enzyme, to which nucleotides bind nonproductively, could account for these results. The measured values of K_{ATP} are complex terms that include the contribution from nonproductive binding of the phosphoryl acceptor and would be dependent on the identity of the phosphoryl acceptor. It would be expected that dissociation constants of the ATP competitive inhibitors could also show phosphoryl acceptor dependence, resulting in a similar potency difference between in vitro and in vivo situations. In other words, inhibitors of LRRK2 currently assessed using peptide substrates may not truly represent efficacy with its physiological substrates. Given the amount of effort currently dedicated to drug discovery targeting LRRK2 kinase, identifying LRRK2 physiological substrates has become even more urgent for potential therapeutic applications in PD, not to mention the importance of elucidating LRRK2's functions.

Inhibition and Isotope Exchange Studies Reveal That the t-G2019S Mutant Follows the Same Kinetic Mechanism as t-wt. The inhibition and isotope exchange patterns rule out a steady-state ordered mechanism and indicate a rapid equilibrium random mechanism for all three reactions catalyzed by t-wt LRRK2 and the t-G2019S mutant. In our previous study, we had determined that full-length mouse wt LRRK2 follows the same rapid equilibrium random mechanism for LRRKtide and PLK-peptide phosphorylation.[19] The results indicate that the truncation of the N-terminus or the source of LRRK2 enzyme does not change the substrate binding order.

There Is a General Base Involved in the Reaction. Linear proton inventories with a small SKIE on the k_{cat} of LRRKtide phosphorylation for both t-wt LRRK2 and the t-G2019S mutant suggest that the rate-limiting step of the process governed by k_{cat} is the product release or any conformational change associated with this process. The use of the proton inventory shape and the size of the solvent isotope effect to determine the number of hydrogenic sites and to diagnose the mechanism have previously been discussed by Schowen and Venkatasubban.[20,36] To understand the catalytic mechanism and to identify the critical residues involved in catalysis, the experiments must be conducted using a rapid-quench instrument to measure the phosphoryl transfer, which is a rapid step. However, here we used the less efficient substrate, LRRKtide^{S}, with the expectation that the 26-fold decrease in k_{cat} would lead to a slow phosphoryl transfer. Proton inventory studies of LRRKtide^{S} phosphorylation revealed a nonlinear dependence of k_n/k_0 on n with an inverse SKIE of 0.7 for both t-wt LRRK2 and the t-G2019S mutant. The reciprocal of the ratio of k_{cat} (k_0/k_n) linearly depends on n. These results suggest that (i) the phosphoryl transfer step is rate-limiting for LRRKtide^{S} phosphorylation and is associated with one proton transfer and (ii) the fractionation factor in the ground state is less than unity.

To make certain that changes in side chain pK_a values in light and heavy water were not causing a dramatic difference in SKIE, we conducted studies of the pL dependence of k_{cat} and k_{cat}/K_m. For LRRKtide^{S} phosphorylation, the pL profile revealed an inverse SKIE on k_{cat} at the optimal pL for both t-wt LRRK2 and the t-G2019S mutant and identified a residue with a pK_a of 7.5. The pK value of the catalytic residue was shifted by 0.5 unit in D_2O, which may result from the solvent equilibrium isotope effect on the residue. Similar results were obtained for k_{cat}/K_m. First, we postulated that SH ionization of a cysteine residue in the active site was the possible source of the low fractionation factor, although a solvent equilibrium isotope effect on the pK value of sulfhydryl group is expected to be 0.15−0.18.[20] To test this hypothesis, we treated t-wt LRRK2 with the cysteine-specific irreversible inhibitor NEM. A dose−response curve was obtained with signs of complete inhibition at high NEM concentrations, suggesting that cysteine residues play an important role in LRRK2 catalysis. Mass spectrometry

analysis revealed that four cysteines (C2010, C2014, C2025, and C2114) in the kinase domain of LRRK2 were modified by NEM to different extents. However, modeling of the kinase domain of the LRRK2−LRRKtide complex revealed no cysteine in the active site; C2101 and C2114 are far from the active site, while C2024 and C2025 are on the catalytic loop of the enzyme. Instead, H1998 was identified in the proximity of the hydroxyl proton of threonine and could function as the possible general base for catalysis. The shift in the p*K* of the catalytic residue by 0.5 unit is consistent with the expected solvent equilibrium isotope effect on p*K* of the histidinyl group of 0.5−0.7.[20] However, it raised the question of the source of the less-than-unity fractionation factor in the ground state. Certainly, the thiol group of cysteine is not the source. In general, a low-barrier hydrogen bond would give rise to such a fractionation factor, and that would be formed only when the p*K* values of the two groups in the hydrogen bond are similar. There are some examples of low-barrier hydrogen bonds for enzyme groups involved in acid−base catalysis.[37] In the case of enolase, the base appears to be a water molecule held between two glutamates.[38] Identification of the source of the low fractionation factor and the general base involved in catalysis will be greatly facilitated by the future elucidation by X-ray crystal structure of the LRRK2 kinase domain. In addition, site-directed mutagenesis may also help elucidate the role and function of H1988 in the future.

Effects of the t-G2019S Mutant on GTPase Activity. The kinetic study of GTP hydrolysis revealed similar kinetic parameters for the t-G2019S mutant and t-wt LRRK2. The t-G2019S mutant does not significantly affect GTP binding and slightly decreases the rate of turnover of GTP to GDP. We have previously reported that binding of GTP or GDP to the GTPase domain does not affect the downstream kinase activity in vitro when the full-length protein purified from mouse brain is used.[35] Those results raised the question of whether LRRK2 undergoes intramolecular regulation in a GTP-dependent manner. In the study presented here, we were still unable to detect any effect of GTP or GDP on kinase activity using truncated proteins. Interestingly, we recently identified a GTPase activating protein that downregulates the kinase activity of LRRK2 by increasing GTPase activity (manuscript in preparation). Those findings constitute direct evidence that LRRK2 requires the GTPase activating protein to undergo intramolecular regulation.

In summary, the studies reported here provide important information for understanding the critical interactions in the active site of LRRK2, which provides an enzymology foundation for assisting in drug discovery efforts for PD. Designing selective kinase inhibitors is a challenge given the fact that all kinases in the TKL subfamily have very similar active sites. The final active site of the enzyme is comprised of residues not only from the kinase but also from the substrate. The identification of critical residues in LRRK2's substrate will provide important information for identifying physiologically relevant substrates of LRRK2 via a consensus motif. The identification of LRRK2's substrates will be critical not only for accurately estimating the efficacy of inhibitors but also for selective inhibitor design.

■ ASSOCIATED CONTENT

Ⓢ Supporting Information

Additional data from initial velocity, inhibition, and pL-dependent studies. This material is available free of charge via the Internet at http://pubs.acs.org.

■ AUTHOR INFORMATION

Corresponding Author

*Laboratory for Drug Discovery in Neurodegeneration, Harvard NeuroDiscovery Center, 65 Landsdowne St., Fourth Floor. Cambridge, MA 02139. Phone: (617) 768-8658. Fax: (617) 768-8606. E-mail: mliu@rics.bwh.harvard.edu (M.L.) or sray@rics.bwh.harvard.edu (S.R.).

Funding

This work was supported by National Institutes of Health Grant 1U24NS049339.

■ ABBREVIATIONS

PD, Parkinson's disease; t-wt LRRK2, truncated wild-type leucine-rich repeat kinase 2; t-G2019S, truncated G2019S mutant; PLK-peptide, PLK-derived peptide with an RRR**S**LLE motif; LRRKtide, RLGRDKYK**T**LRQIRQ; LRRKtide^S, RLGRDKYK**S**LRQIRQ.

■ REFERENCES

(1) Moore, D. J., West, A. B., Dawson, V. L., and Dawson, T. M. (2005) Molecular pathophysiology of Parkinson's disease. *Annu. Rev. Neurosci. 28*, 57−87.

(2) Paisan-Ruiz, C., Jain, S., Evans, E. W., Gilks, W. P., Simon, J., van der Brug, M., Lopez de Munain, A., Aparicio, S., Gil, A. M., Khan, N., Johnson, J., Martinez, J. R., Nicholl, D., Carrera, I. M., Pena, A. S., de Silva, R., Lees, A., Marti-Masso, J. F., Perez-Tur, J., Wood, N. W., and Singleton, A. B. (2004) Cloning of the gene containing mutations that cause PARK8-linked Parkinson's disease. *Neuron 44*, 595−600.

(3) Zimprich, A., Biskup, S., Leitner, P., Lichtner, P., Farrer, M., Lincoln, S., Kachergus, J., Hulihan, M., Uitti, R. J., Calne, D. B., Stoessl, A. J., Pfeiffer, R. F., Patenge, N., Carbajal, I. C., Vieregge, P., Asmus, F., Muller-Myhsok, B., Dickson, D. W., Meitinger, T., Strom, T. M., Wszolek, Z. K., and Gasser, T. (2004) Mutations in LRRK2 cause autosomal-dominant parkinsonism with pleomorphic pathology. *Neuron 44*, 601−607.

(4) Berg, D., Schweitzer, K. J., Leitner, P., Zimprich, A., Lichtner, P., Belcredi, P., Brussel, T., Schulte, C., Maass, S., Nagele, T., Wszolek, Z. K., and Gasser, T. (2005) Type and frequency of mutations in the LRRK2 gene in familial and sporadic Parkinson's disease. *Brain 128*, 3000−3011.

(5) Khan, N. L., Jain, S., Lynch, J. M., Pavese, N., Abou-Sleiman, P., Holton, J. L., Healy, D. G., Gilks, W. P., Sweeney, M. G., Ganguly, M., Gibbons, V., Gandhi, S., Vaughan, J., Eunson, L. H., Katzenschlager, R., Gayton, J., Lennox, G., Revesz, T., Nicholl, D., Bhatia, K. P., Quinn, N., Brooks, D., Lees, A. J., Davis, M. B., Piccini, P., Singleton, A. B., and Wood, N. W. (2005) Mutations in the gene LRRK2 encoding dardarin (PARK8) cause familial Parkinson's disease: Clinical, pathological, olfactory and functional imaging and genetic data. *Brain 128*, 2786−2796.

(6) Farrer, M., Stone, J., Mata, I. F., Lincoln, S., Kachergus, J., Hulihan, M., Strain, K. J., and Maraganore, D. M. (2005) LRRK2 mutations in Parkinson disease. *Neurology 65*, 738−740.

(7) Smith, W. W., Pei, Z., Jiang, H., Dawson, V. L., Dawson, T. M., and Ross, C. A. (2006) Kinase activity of mutant LRRK2 mediates neuronal toxicity. *Nat. Neurosci. 9*, 1231−1233.

(8) Greggio, E., Jain, S., Kingsbury, A., Bandopadhyay, R., Lewis, P., Kaganovich, A., van der Brug, M. P., Beilina, A., Blackinton, J., Thomas, K. J., Ahmad, R., Miller, D. W., Kesavapany, S., Singleton, A., Lees, A., Harvey, R. J., Harvey, K., and Cookson, M. R. (2006) Kinase

activity is required for the toxic effects of mutant LRRK2/dardarin. *Neurobiol. Dis. 23*, 329−341.
(9) Guo, L., Gandhi, P. N., Wang, W., Petersen, R. B., Wilson-Delfosse, A. L., and Chen, S. G. (2007) The Parkinson's disease-associated protein, leucine-rich repeat kinase 2 (LRRK2), is an authentic GTPase that stimulates kinase activity. *Exp. Cell Res. 313*, 3658−3670.
(10) Ito, G., Okai, T., Fujino, G., Takeda, K., Ichijo, H., Katada, T., and Iwatsubo, T. (2007) GTP binding is essential to the protein kinase activity of LRRK2, a causative gene product for familial Parkinson's disease. *Biochemistry 46*, 1380−1388.
(11) West, A. B., Moore, D. J., Biskup, S., Bugayenko, A., Smith, W. W., Ross, C. A., Dawson, V. L., and Dawson, T. M. (2005) Parkinson's disease-associated mutations in leucine-rich repeat kinase 2 augment kinase activity. *Proc. Natl. Acad. Sci. U.S.A. 102*, 16842−16847.
(12) West, A. B., Moore, D. J., Choi, C., Andrabi, S. A., Li, X., Dikeman, D., Biskup, S., Zhang, Z., Lim, K. L., Dawson, V. L., and Dawson, T. M. (2007) Parkinson's disease-associated mutations in LRRK2 link enhanced GTP-binding and kinase activities to neuronal toxicity. *Hum. Mol. Genet. 16*, 223−232.
(13) Xiong, Y., Coombes, C. E., Kilaru, A., Li, X., Gitler, A. D., Bowers, W. J., Dawson, V. L., Dawson, T. M., and Moore, D. J. (2010) GTPase activity plays a key role in the pathobiology of LRRK2. *PLoS Genet. 6*, e1000902.
(14) Lee, B. D., Shin, J. H., VanKampen, J., Petrucelli, L., West, A. B., Ko, H. S., Lee, Y. I., Maguire-Zeiss, K. A., Bowers, W. J., Federoff, H. J., Dawson, V. L., and Dawson, T. M. (2010) Inhibitors of leucine-rich repeat kinase-2 protect against models of Parkinson's disease. *Nat. Med. 16*, 998−1000.
(15) Eswar, N., Eramian, D., Webb, B., Shen, M. Y., and Sali, A. (2008) Protein structure modeling with MODELLER. *Methods Mol. Biol. 426*, 145−159.
(16) Vaguine, A. A., Richelle, J., and Wodak, S. J. (1999) SFCHECK: A unified set of procedures for evaluating the quality of macromolecular structure-factor data and their agreement with the atomic model. *Acta Crystallogr. D55*, 191−205.
(17) Verind, G. (1996) WHAT IF: A molecular modeling and drug design program. *J. Mol. Graphics 8*, 52−56.
(18) Segel, I. H. N. (1975) *Enzyme Kinetics*, John Wiley & Sons, New York.
(19) Liu, M., Poulose, S., Schuman, E., Zaitsev, A. D., Dobson, B., Auerbach, K., Seyb, K., Cuny, G. D., Glicksman, M. A., Stein, R. L., and Yue, Z. (2010) Development of a mechanism-based high-throughput screen assay for leucine-rich repeat kinase 2: Discovery of LRRK2 inhibitors. *Anal. Biochem. 404*, 186−192.
(20) Schowen, K. B., and Schowen, R. L. (1982) Solvent isotope effects of enzyme systems. *Methods Enzymol. 87*, 551−606.
(21) Friesner, R. A., Banks, J. L., Murphy, R. B., Halgren, T. A., Klicic, J. J., Mainz, D. T., Repasky, M. P., Knoll, E. H., Shelley, M., Perry, J. K., Shaw, D. E., Francis, P., and Shenkin, P. S. (2004) Glide: A new approach for rapid, accurate docking and scoring. 1. Method and assessment of docking accuracy. *J. Med. Chem. 47*, 1739−1749.
(22) Halgren, T. A., Murphy, R. B., Friesner, R. A., Beard, H. S., Frye, L. L., Pollard, W. T., and Banks, J. L. (2004) Glide: a new approach for rapid, accurate docking and scoring. 2. Enrichment factors in database screening. *J. Med. Chem. 47*, 1750−1759.
(23) Gosal, D., Ross, O. A., Wiley, J., Irvine, G. B., Johnston, J. A., Toft, M., Mata, I. F., Kachergus, J., Hulihan, M., Taylor, J. P., Lincoln, S. J., Farrer, M. J., Lynch, T., and Mark Gibson, J. (2005) Clinical traits of LRRK2-associated Parkinson's disease in Ireland: A link between familial and idiopathic PD. *Parkinsonism Relat. Disord. 11*, 349−352.
(24) Kannan, N., and Neuwald, A. F. (2005) Did protein kinase regulatory mechanisms evolve through elaboration of a simple structural component? *J. Mol. Biol. 351*, 956−972.
(25) Kornev, A. P., Haste, N. M., Taylor, S. S., and Eyck, L. F. (2006) Surface comparison of active and inactive protein kinases identifies a conserved activation mechanism. *Proc. Natl. Acad. Sci. U.S.A. 103*, 17783−17788.
(26) Kornev, A. P., Taylor, S. S., and Ten Eyck, L. F. (2008) A helix scaffold for the assembly of active protein kinases. *Proc. Natl. Acad. Sci. U.S.A. 105*, 14377−14382.
(27) Hemmer, W., McGlone, M., Tsigelny, I., and Taylor, S. S. (1997) Role of the glycine triad in the ATP-binding site of cAMP-dependent protein kinase. *J. Biol. Chem. 272*, 16946−16954.
(28) Parisiadou, L., Xie, C., Cho, H. J., Lin, X., Gu, X. L., Long, C. X., Lobbestael, E., Baekelandt, V., Taymans, J. M., Sun, L., and Cai, H. (2009) Phosphorylation of ezrin/radixin/moesin proteins by LRRK2 promotes the rearrangement of actin cytoskeleton in neuronal morphogenesis. *J. Neurosci. 29*, 13971−13980.
(29) Gillardon, F. (2009) Leucine-rich repeat kinase 2 phosphorylates brain tubulin-β isoforms and modulates microtubule stability: A point of convergence in parkinsonian neurodegeneration? *J. Neurochem. 110*, 1514−1522.
(30) Imai, Y., Gehrke, S., Wang, H. Q., Takahashi, R., Hasegawa, K., Oota, E., and Lu, B. (2008) Phosphorylation of 4E-BP by LRRK2 affects the maintenance of dopaminergic neurons in *Drosophila*. *EMBO J. 27*, 2432−2443.
(31) Gloeckner, C. J., Schumacher, A., Boldt, K., and Ueffing, M. (2009) The Parkinson disease-associated protein kinase LRRK2 exhibits MAPKKK activity and phosphorylates MKK3/6 and MKK4/7, in vitro. *J. Neurochem. 109*, 959−968.
(32) Hsu, C. H., Chan, D., Greggio, E., Saha, S., Guillily, M. D., Ferree, A., Raghavan, K., Shen, G. C., Segal, L., Ryu, H., Cookson, M. R., and Wolozin, B. (2010) MKK6 binds and regulates expression of Parkinson's disease-related protein LRRK2. *J. Neurochem. 112*, 1593−1604.
(33) Nichols, R. J., Dzamko, N., Morrice, N. A., Campbell, D. G., Deak, M., Ordureau, A., Macartney, T., Tong, Y., Shen, J., Prescott, A. R., and Alessi, D. R. (2010) 14-3-3 binding to LRRK2 is disrupted by multiple Parkinson's disease-associated mutations and regulates cytoplasmic localization. *Biochem. J. 430*, 393−404.
(34) Nichols, R. J., Dzamko, N., Hutti, J. E., Cantley, L. C., Deak, M., Moran, J., Bamborough, P., Reith, A. D., and Alessi, D. R. (2009) Substrate specificity and inhibitors of LRRK2, a protein kinase mutated in Parkinson's disease. *Biochem. J. 424*, 47−60.
(35) Liu, M., Dobson, B., Glicksman, M. A., Yue, Z., and Stein, R. L. (2010) Kinetic mechanistic studies of wild-type leucine-rich repeat kinase 2: Characterization of the kinase and GTPase activities. *Biochemistry 49*, 2008−2017.
(36) Venkatasubban, K. S., and Schowen, R. L. (1984) The proton inventory technique. *CRC Crit. Rev. Biochem. 17*, 1−44.
(37) Cleland, W. W. (1992) Low-barrier hydrogen bonds and low fractionation factor bases in enzymatic reactions. *Biochemistry 31*, 317−319.
(38) Lebioda, L., and Stec, B. (1991) Mechanism of enolase: The crystal structure of enolase-Mg^{2+}-2-phosphoglycerate/phosphoenol-pyruvate complex at 2.2-Å resolution. *Biochemistry 30*, 2817−2822.